Investigation of the unsteady pressure pulsations in the prototype Francis turbines during load variation and startup

Chirag Trivedi, Peter Joachim Gogstad, and Ole Gunnar Dahlhaug

Citation: Journal of Renewable and Sustainable Energy **9**, 064502 (2017);
View online: https://doi.org/10.1063/1.4994884
View Table of Contents: http://aip.scitation.org/toc/rse/9/6
Published by the American Institute of Physics

Investigation of the unsteady pressure pulsations in the prototype Francis turbines during load variation and startup

Chirag Trivedi,[a] Peter Joachim Gogstad, and Ole Gunnar Dahlhaug
Norwegian University of Science and Technology (NTNU), NO-7491 Trondheim, Norway

(Received 8 July 2017; accepted 27 November 2017; published online 18 December 2017)

This work investigates the unsteady pressure fluctuations in two prototype Francis turbines during load variation and start-up. Although hydraulic turbines are expected to experience such events over their lifetime, the resulting pressure amplitudes are so significant that they take a toll on a machine's operating life. The interest of the present study is to experimentally measure and numerically characterize time-dependent pressure pulsations. Specific focus is on (1) how pressure pulsations of both synchronous and asynchronous types in vertical- and horizontal-axis turbines change when the load of a turbine changes from steady conditions, (2) what the pressure amplitudes during load change are, and (3) how quickly pressure amplitudes vary when a generator is synchronized to the power grid (load) during start-up. To this end, four pressure sensors were integrated in the draft tube cone. The results are quite interesting, especially during transition from the steady state to the transient load change. In the vertical-axis turbine, amplitudes of asynchronous pressure pulsations are 20 times larger than those of the synchronous component; whereas, in the horizontal-axis turbine, amplitudes of asynchronous pressure pulsations are two times smaller than those of the synchronous component. During a load change, amplitudes of synchronous pressure pulsations are nearly double compared with the asynchronous component. For the turbine startup, only synchronous-type pressure pulsations are found and the flow was asymmetrical over the draft tube circumference. *Published by AIP Publishing*. https://doi.org/10.1063/1.4994884

I. INTRODUCTION

Today, both continual and intermittent energy resources are used for electricity supply. Continual types of energy sources guarantee electricity continuously and intermittent types of energy sources do not. The variations in the electricity demand and generation often disrupt the grid network, which affects the constant supply of electricity to the end users. Due to their flexibility in changing the power output within the shortest possible time, hydraulic turbines have been widely used to meet real-time electricity demand.[1–3] The turbines pass through transient cycles, such as load acceptance (LA), load rejection (LR), start-up, shutdown, and total load rejection during the power grid stabilization.[4] Furthermore, hydraulic turbines experience unstable flow conditions and high amplitude pressure pulsations during the transient cycles.[5–10] The pressure amplitudes are primarily dependent on the instantaneous rate of the guide vanes' movements and the runner's speed.[11,12]

For the load acceptance cycle, the power output from the hydraulic turbine increases by opening the guide vanes. The guide vanes are operated through a governing system based on the power required to balance the grid parameters. For the load rejection cycle, the discharge to the runner is decreased by closing the guide vanes. During the load acceptance and rejection cycles, the generator is connected to the grid network and operated at a constant (synchronous)

[a]Author to whom correspondence should be addressed: chirag.trivedi@ntnu.no. Tel.: +47 735 93849.

speed. For the start-up cycle, the guide vanes are initially opened by a few percentages from a completely closed position. As the discharge to the runner increases, the runner starts spinning at a synchronous speed to that of the corresponding turbine. The generator then is coupled to the grid network at a minimum load. After synchronization, the power output is further increased to the set value by increasing the discharge to the runner.

Unsteady pressure measurements observed during the transient cycles of a Francis turbine model indicated that a turbine could experience more than twice the pressure amplitudes observed at the best efficiency point (BEP).[13–15] Pressure measurements in a draft tube indicated that high amplitude pressure oscillations occur during the load variation and start-stop cycles. The oscillations were nearly three times higher than that of the normal operating conditions. The literature indicated that the repeated transients affect the operating life of the turbine components.[16–19] During a transient condition, the turbine passes through a rapid pressure variation and experiences low-cycle fatigue.[20,21] The repeated fatigue loading to the runner blades initiate cracks where the blades are welded.[22]

Pressure pulsations developed in a draft tube are primarily related to the vortex breakdown. The pressure pulsations are composed of two different phenomena that occur simultaneously at the same frequency, which may be synchronous (axial) and asynchronous (radial) types.[23,24] The synchronous component may have equal phase and amplitude in the runner and the draft tube. The pressure may be considered as a plane wave propagating to the hydraulic system through the draft tube. The asynchronous component is a pressure pattern that develops at the runner downstream and that rotates about the circumference of the draft tube. The rotation period is dependent on the circumference and the runner angular speed. The synchronous component may not be present at high load conditions. In a straight/conical draft tube, only asynchronous type pulsations exist.[25]

Both synchronous and asynchronous types of pressure pulsations cause different impacts on turbine operation. It is important to analyze and distinguish such pulsations properly. During the steady-state operating condition of a turbine, the pulsations are periodic and may repeat over certain periods of time.[26–29] However, during load variation and start-stop, the pressure pulsations are non-repeating and largely dependent on the runner's instantaneous speed as well as guide vanes' apertures at that time. Recently, velocity measurement conducted by Goyal *et al.*[30,31] indicated that the vortex structure in the draft tube evolves over a certain time as the runner accelerates/decelerates. The study showed that, unlike a steady-state load,[32–35] amplitudes of both types of pressure pulsations vary with time as the load changes from one operating point to another. The frequency of synchronous pulsations appeared before the asynchronous pulsations during load variation from or to part load. Axial velocity of flow leads the synchronous type and the radial velocity leads the asynchronous type pulsations during formation of the vortex rope as load changes from BEP to part load.

So far, the investigations were focused on steady-state operating conditions of the turbine, and very few investigations have been performed on the transient operating conditions. Among them, the majority focused on the model Francis turbine. Previous investigations[36–38] clearly indicated that the realistic prototype measurements are vital to obtain reliable information on how unsteady pressure pulsations and their synchronous-asynchronous component vary during load variation and start-stop. Because, while investigating the transient conditions on model turbines, there are certain limitations, such as effects of water hammer[39,40] and draft tube surge,[41,42] that are not produced perfectly for the prototype conditions. Furthermore, variation in frequencies of standing waves due to hydroacoustic phenomena[43,44] and associated speed of sound[45,46] are not captured very well. Transient measurements on prototypes are rarely conducted (except commissioning time) and generally are not published due to limited access to prototypes, production losses, and confidentiality. The present work is aimed to investigate the pressure loading in two prototype turbines during transient operating conditions, such as load acceptance, load rejection, and start-up. The focus is to investigate the unsteady pressure amplitudes at different locations in the draft tube and how synchronous and asynchronous components vary with time. The paper is structured as follows: turbines instrumentation, and uncertainty quantification are described in Sec. II; Sec. III is divided into two parts: turbine-1, i.e., vertical-axis

prototype Francis turbine; turbine-2, i.e., horizontal-axis prototype Francis turbine; and key findings are listed in Sec. IV.

II. MATERIALS AND METHODS

A. Measurements

The pressure measurements were performed on two medium head Francis turbines located in Leirfossen, Trondheim, Norway. The Francis turbine (turbine-1), located at Nedre Leirfossen, was a vertical-axis turbine. Another Francis turbine (turbine-2), located at Øvre Leirfossen, was a horizontal-axis turbine. Figure 1 presents a two-dimensional view of the Francis turbine located at Øvre Leirfossen. Table I presents the operating parameters of both turbines observed at the BEP. The speed factor (n_{ED}), discharge factor (Q_{ED}), and specific speed (N_{QE}) are estimated by using Eqs. (1), (2), and (3), respectively,[47]

$$n_{ED} = \frac{n \cdot D}{E^{0.5}}, \tag{1}$$

$$Q_{ED} = \frac{Q}{D^2 \cdot E^{0.5}}, \tag{2}$$

$$N_{QE} = \frac{n \cdot Q^{0.5}}{E^{0.75}}, \tag{3}$$

where n is the runner's angular speed in revolutions per second (rps); D is the runner's outlet diameter in m; Q is the discharge in $m^3\ s^{-1}$; and E is the specific hydraulic energy in J kg^{-1}. The specific speed, N_{QE}, of both the turbines is 0.27. The runner's outlet diameters of turbine-1 and turbine-2 are 1.389 and 1.334 m, respectively. Both turbines include 8 stay vanes, 16 guide vanes, and 13 blades.

The unsteady pressure measurements in the draft tube cone were obtained by using four PTX 610 pressure transmitters; the operating range was 0–250 kPa absolute. There were four pressure taps on the draft tube cone, and each tap was 90° circumferentially apart from each other on the same cross-section ($0.27 \cdot D$ from the runner's outlet). Sensors S1 and S3 were in

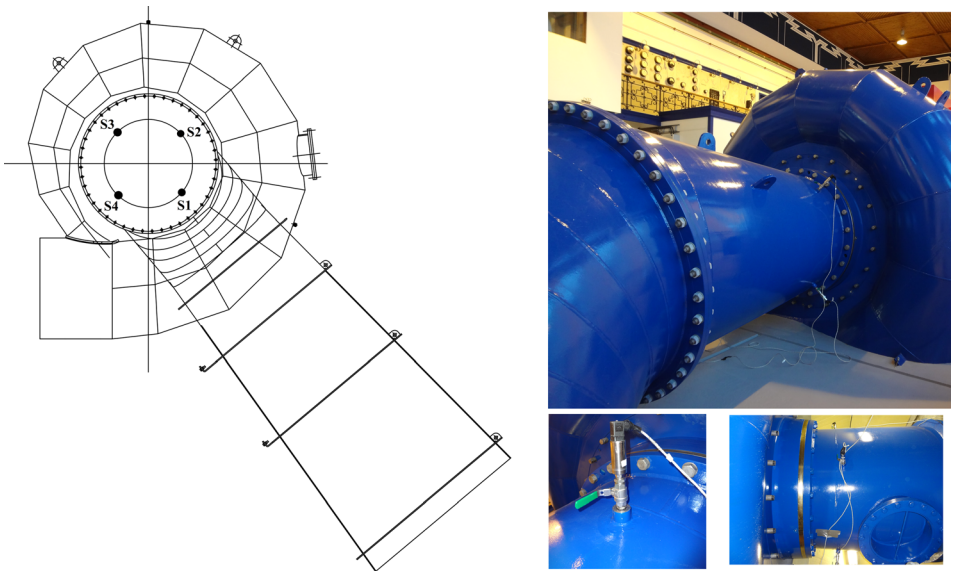

FIG. 1. Two-dimensional view of a Francis turbine (horizontal axis) prototype located at Øvre Leirfossen, Trondheim, Norway. S1, S2, S3, and S4 are the locations of the pressure sensors in the draft tube cone. Photographs on the right-hand side indicate the physical locations of the pressure sensors.

TABLE I. Operating parameters of the investigated Francis turbines.

Parameter (symbol)	Turbine-1	Turbine-2	Unit
Head (H)	25.7	32.6	m
Discharge (Q)	10	10.5	$m^3\ s^{-1}$
Power (P)	2.5	3.5	MW
Efficiency (η)	94.7	91.7	%
Angular speed (n)	5.55	6.25	rps
Runner outlet diameter (D)	1.389	1.334	m
Speed factor (n_{ED})	0.48	0.47	…
Discharge factor (Q_{ED})	0.33	0.33	…
Specific speed (N_{QE})	0.274	0.270	…
Runner axis	Vertical	Horizontal	…

line with the draft tube outlet axis. S2 and S4 were perpendicular to S1 and S3, respectively. Before the prototype measurements, the pressure sensors were calibrated thoroughly in the Waterpower Laboratory. Table II presents the range of parameters on transient measurements, load acceptance, load rejection, and start-up. For turbine-1, two transient conditions of load acceptance and two transient conditions of load rejection were measured. For turbine-2, three transient conditions of load acceptance were measured. Turbine start-up to 40% load measurements were performed on both turbines. The time for a 20% load change was approximately 12 s for both turbines; for start-up, the time was approximately 27 s. For turbine-2, the start-up time was long (162 s) due to pressure balance across the turbine and waiting for the generator synchronization. The pressure data were acquired by using a National Instrument (NI) data acquisition system and the LabVIEW program. The data were sampled at a sampling rate of 2.5 kHz. The sampling rate was defined by an in-built filter in the NI module to avoid the aliasing effect and when considering the maximum possible frequency in the draft tube, i.e., 10 harmonics of the blade-passing frequency within the anti-aliasing range (sampling rate/2). The frequency resolution was sufficient (less than 0.05% of the runner's angular speed) to obtain a small variation of frequency in the time domain. In this paper, the load is presented as a percentage of the BEP load; BEP is considered as a 100% load.

III. RESULTS AND DISCUSSION

A. Pressure measurements: Turbine-1

1. Load acceptance and load rejection

Turbine-1 is a vertical-axis type and the draft tube was an elbow type. Pressure data acquired from the S1, S2, S3, and S4 locations were analyzed for all transient conditions. Due to the large volume of experimental data and the similarity in the average pressure variation at

TABLE II. Transient cycles and operating points of the pressure measurements; a 100% load corresponds to the BEP operating condition.

Transient cycle	Turbine-1 (Nedre Leirfossen)	Turbine-2 (Øvre Leirfossen)
Load acceptance (LA)	50%–70% load (12 s)	70%–90% load (11 s)
	90%–110% load (13 s)	90%–100% load (7 s)
		100%–110% load (7 s)
Load rejection (LR)	100%–50% load (19 s)	…
	110%–100% load (7 s)	
Start-up	0%–40% load (27 s)	0%–40% load (162 s)

all locations, detailed analysis at one of the locations, is elaborated. However, to investigate the synchronous and asynchronous pulsations, data of all the sensor locations are presented. Figure 2 depicts the pressure variation at S1 during the transient cycles of load acceptance (LA) and load rejection (LR). The load acceptance is performed by increasing the power output from a 50% to a 70% load and a 90% to a 110% load. The load rejection is performed by decreasing the power output from a 100% to 50% load and a 110% to 100% load. During the load acceptance, pressure in the draft tube decreases, and, during load rejection, the pressure increases. However, for the 50%–70% load acceptance, the change of pressure is very small (0.3 kPa). The pressure pulsations are presented for a time of 200 s, and the start time of the transient cycles is adjusted to 50 s for all the cases. The mean pressure values are averaged over a window length of 3 s for the corresponding operating conditions. To visualize the pressure pulsations during the transition from one operating point to another, enlarged (zoom) windows of 25 s, i.e., $t = 50$–75 s, are illustrated beside the corresponding figures. A zoom window, Fig. 2(b), depicts the variation in frequency and amplitude of the unsteady pressure pulsation. High-amplitude pressure pulsations can be observed from 55 s and 60 s, which may be associated with a frequency of the vortex rope in the draft tube. At a 50% load, the random pulsations are dominant; whereas, at 70% load systematic pulsations, vortex rope, and rotor stator interaction, are dominant. Another transient cycle of load acceptance from a 90% to a 110% load is provided in Figs. 2(c) and 2(d). A pressure drop from 85.2 kPa to 81.8 kPa can be seen during the

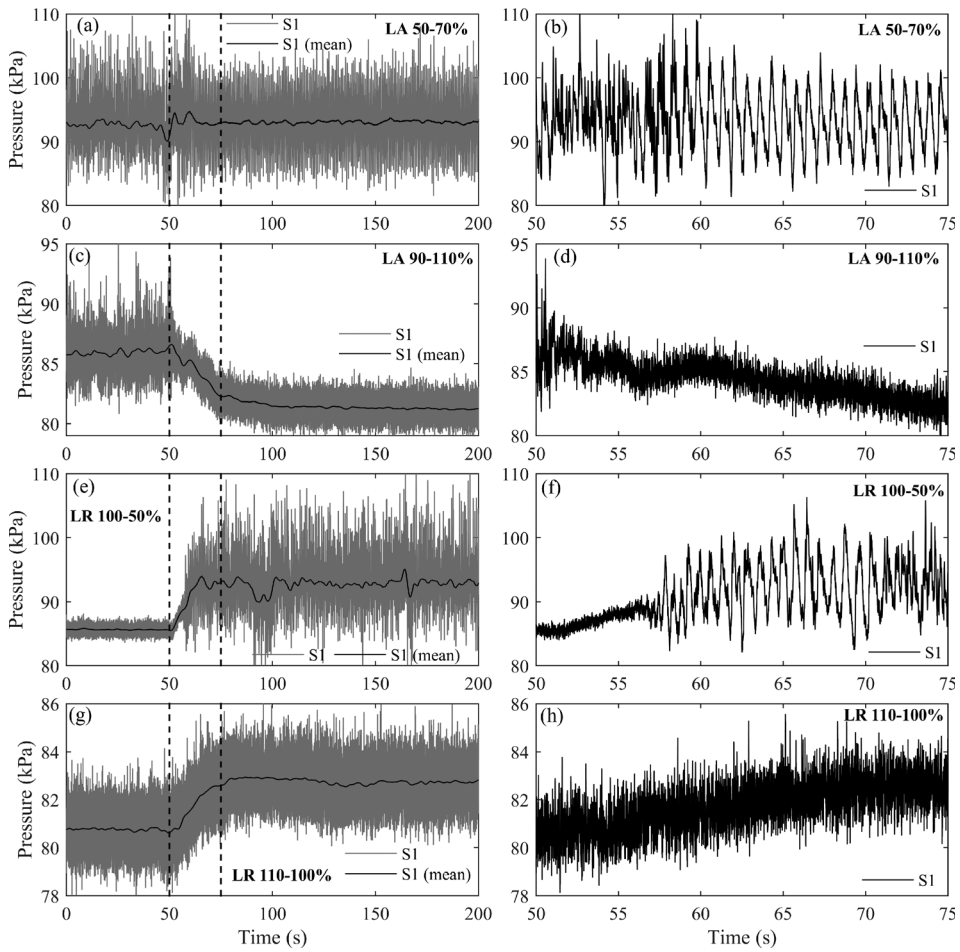

FIG. 2. Pressure variation during load acceptance (LA) and load rejection (LR) at S1; the figures on the left side depict a full scale of the pressure variation, starting from the initial operating point to the final operating point of the load acceptance or load rejection cycles; and figures on the right side depict the pressure pulsations in a zoomed-in window of the corresponding transient cycle.

transient period, and the pressure drop is equivalent to head of 0.35 m. At the 90% load operating condition, the amplitudes of the pressure pulsations are nearly two times larger compared with the amplitudes observed at the 110% load operating condition. The load rejection cycle from a 100% (BEP) to a 50% load is provided in Figs. 2(e) and 2(f). At a 100% load, the amplitude of the pressure pulsations is small, which is a stable flow condition in the draft tube. The amplitudes increase as the transition from a 100% load occurs, and the amplitudes are nearly five times larger at a 50% load. The transition to the unstable condition occurs at approximately 58 s, and the pressure amplitudes slowly increase. The maximum amplitudes can be observed between 65 s and 70 s when the operating load is approximately 70%. The amplitudes slowly decrease after 70 s when the turbine reaches a 50% load operating condition. The load rejection from a 110% to a 100% load is presented in Figs. 2(g) and 2(h). The pressure amplitudes at the 110% load are 0.2 kPa larger compared with the amplitudes observed at the 100% load. No significant variation was observed during this transient cycle. Operating points $\pm 10\%$ of the BEP seem stable in this turbine. A similar variation was observed for the other locations, i.e., S2, S3, and S4. Therefore, the pressure data at these locations are not shown.

The time-series pressure signal usually contains frequencies related to the developed flow phenomena and random noise. It is difficult to distinguish the pressure pulsations related to flow phenomena when the amplitudes are quite similar to random noise. Techniques available in the MATLAB software were applied to estimate the noise component. The signal-to-noise ratio (SNR) analysis was performed on the acquired data from the pressure sensors. Equation (6) was used to calculate the SNR,

$$\mathrm{SNR_{dB}} = 10 \log_{10}\left(\frac{P_{\mathrm{signal}}}{P_{\mathrm{noise}}}\right) \quad (\mathrm{dB}), \tag{4}$$

where P_{signal} and P_{noise} are the powers of the input signal (frequencies related to the vortex breakdown and the runner angular speed) and random noise, respectively. Table III shows the relative noise power (power of random pressure fluctuations) in the pressure signals for different operating loads. The estimated noise power (dB) is normalized by the corresponding noise power (dB) at a 100% load. It can be seen that the noise power at the 50% and 90% load dominant. At the 50% load, the random noise was observed between 0.6 and 80 Hz; whereas, at the 90% load, the random noise was observed between 0.4 and 32 Hz. Low-noise power at a 70% load is due to high signal power associated with the vortex rope frequency. At a 90%, 100%, and 110% load, the dominant signal power was attributed with the blade-passing frequency of 72 Hz.

The change in the amplitudes of the unsteady pressure pulsations during the transient cycle may be explained by a time-average standard deviation. The time-average standard deviation of the pressure pulsations during the load acceptance and load rejection cycles is presented in Fig. 3. The time-dependent standard deviation was computed by using pressure data of 0.1-s window segment and 50% overlapping.[48] The standard deviation corresponds to variation from the mean pressure value. The transient start time is adjusted to 50 s. The highest standard deviation is observed for a load acceptance from the 50% to 70% load. At the 50% load, the standard deviation is 3.8 kPa, which increases to 5.4 kPa (equivalent to 2.14% of the operating

TABLE III. Relative noise power in pressure signals S1, S2, S3, and S4 for different operating loads of the turbine; the noise power is normalized by the noise power at the 100% load operating condition.

Location	50% load	70% load	90% load	100% load	110% load
S1	2.64	1.07	1.57	1	1.21
S2	2.61	1.02	1.59	1	1.28
S3	2.66	1.18	1.63	1	1.27
S4	2.59	1.12	1.58	1	1.29

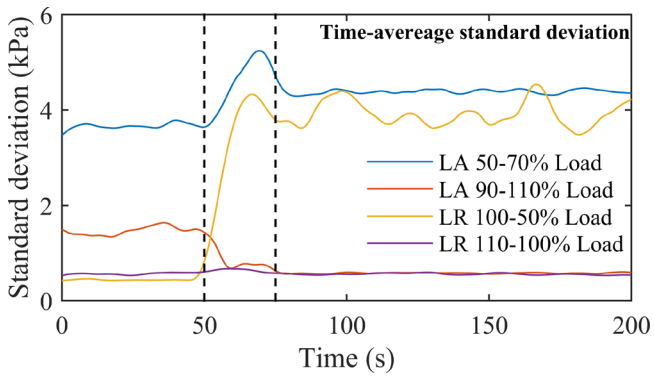

FIG. 3. The time-average standard deviation of the pressure pulsations during the load acceptance and load rejection cycles of a Francis turbine (turbine-1); the dotted lines at 50 s and 75 s indicate the time of the transient cycles.

head) as the load increases to 70%. The steady-state value of the standard deviation at the 70% load is observed after 60 s. A similar variation can be observed for the load rejection from the 100% to 50% load operating condition. At the 100% load operating condition, the standard deviation is less than 0.8 kPa, which increases with discharge and nearly stabilizes at 3.8 kPa (equivalent to 1.51% of head). The estimated standard deviations for 50%, 70%, 90%, 100%, and 110% load operating conditions are 3.8 kPa, 5.4 kPa, 1.7 kPa, 0.8 kPa, and 1 kPa, respectively.

A time-domain spectral analysis was conducted to investigate the frequency components and corresponding amplitudes in the acquired pressure data. Figure 4 presents a prepared spectrogram of the unsteady pressure data acquired from S1 during the load acceptance from the 50% to the 70% load. The instantaneous variation in the frequencies and amplitudes during the transient cycle is presented. The frequencies are normalized by using Eq. (4);

$$f^* = \frac{f}{n}, \tag{5}$$

where f is the frequency component in Hz; and n is the runner angular speed (synchronous speed) in rps or Hz. The amplitudes are normalized by using Eq. (5) as follows:

$$\tilde{p}_{\mathrm{E\,rms}} = \frac{p - p_{\mathrm{rms}}}{(\rho \cdot E)_{\mathrm{BEP}}}, \tag{6}$$

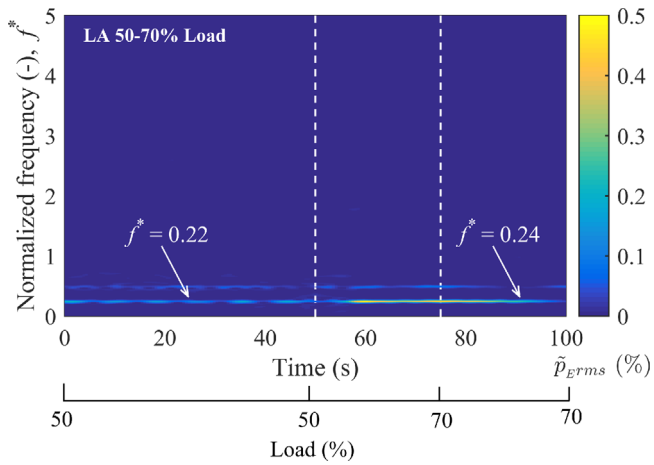

FIG. 4. A spectrogram of the time-series pressure pulsation at S1 during load acceptance from a 50% to a 70% load. The dotted lines at 50 s and 75 s indicate the time of the transient cycles. The frequencies are normalized by the runner's angular speed of 5.55 Hz. The amplitudes are normalized by the reference pressure observed at the BEP: $\rho{\cdot}E = 252.17$ kPa.

where p is the pressure value acquired during the transient condition in kPa; p_{rms} is the time-average root-mean-square value of the corresponding pressure signal in kPa; and $\rho{\cdot}E$ is the reference pressure observed at the BEP in kPa. To perform time-dependent power spectral analysis, a window size of 0.5 s with 80% overlap was selected.[49] A normalized frequency of 0.22 and its harmonic can be clearly observed during load acceptance from a 50% to a 70% load. The frequencies correspond to the vortex rope in the draft tube. Interestingly, the vortex rope frequency $f^* = 0.22$ gradually changes to $f^* = 0.24$ as the load changes from 50% to 70% at approximately 60 s, and the amplitudes also increase, as discussed in Fig. 2(b). At a steady 50% load, amplitudes of frequency 0.22 are inconsistent and repeated in a cyclic pattern. During the transition, the amplitudes increase as random pulsations disappeared and the pulsations associated with vortex rope frequency organized after achieving a 70% load. Figure 5 presents a spectrogram of the unsteady pressure pulsations at S1 during load rejection from a 100% to a 50% load. The transition between 50 s and 75 s indicates how the frequency that corresponds to the vortex rope becomes apparent. A bright mark at the normalized frequency of 0.22 can be observed at 60 s, which corresponds to the formation of the vortex rope, when the transition occurs from the stable flow condition to the unstable flow condition to a 70% load and then a 50% load. The amplitude of the vortex rope frequency decreases when the load is approximately 60% and the amplitudes remain small; at the same time, amplitudes of random pressure fluctuations increase. The resulting amplitudes of the random fluctuations are nearly the same as the vortex rope. The increase of random fluctuations may be associated with the development of vortical flow in the blade passages, which travel to the draft tube. Unlike a 70% load, vortical flow leaving the runner blades may not be organized around the runner cone/hub/axis of rotation. As the load changes from a 70% load to a 50% load, tangential (whirl component) velocity of the flow increases as well as the effect of centrifugal force. The vortical flow is directed towards the runner band or draft tube circumference, and the vortical flow is no longer organized around the runner axis. Furthermore, recirculating flow in the draft tube may also contribute to developing random fluctuations.

The pressure pulsations in the draft tube are composed of systematic and random types. The systematic pulsations are associated with the certain flow phenomena and the frequency of the hydroacoustic effect. The random pulsations may be associated with the random noise, turbulent flow noise, or random vibration of the structure. In the draft tube, the dominant pressure pulsations are related to the vortex rope under the off-design operating conditions. The systematic pulsations may be reasonably explained by making a distinction between the synchronous (axial) and asynchronous (radial) pressure pulsations.[50,51] The procedure suggested in the literature[23,52] are used to determine the synchronous and asynchronous components in the acquired

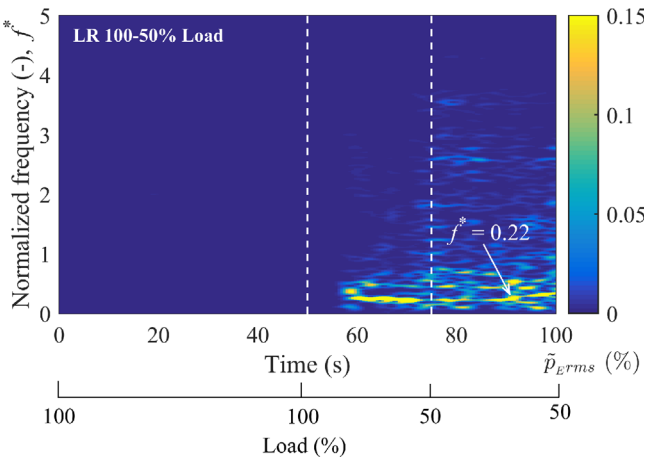

FIG. 5. A spectrogram of the time-series pressure pulsation at S1 during load rejection from a 100% to a 50% load. The dotted lines at 50 s and 75 s indicate the time of the transient cycles. The frequencies are normalized by the runner's angular speed of 5.55 Hz. The amplitudes are normalized by the reference pressure observed at the BEP: $\rho{\cdot}E = 252.17$ kPa.

pressure data. Equations (6) and (7) can be used to estimate the synchronous and asynchronous components, respectively, in the corresponding transient cycle,

$$\tilde{p}_{\text{syn}} = \frac{\tilde{p}_{S1} + \tilde{p}_{S3}}{2} \quad (\text{kPa}), \tag{7}$$

$$\tilde{p}_{\text{asyn}} = \frac{\tilde{p}_{S1} - \tilde{p}_{S3}}{2} \quad (\text{kPa}), \tag{8}$$

where $\tilde{p}$ is the fluctuating pressure acquired from the sensor locations. Figure 6 illustrates the spectral analysis of the pressure data acquired from locations S1 and S3 during load acceptance from the 50% to 70% load operating condition. The normalized frequencies related to the vortex rope are 0.22 and 0.24 at 50% and 70% load operating conditions, respectively. Figure 6(a) presents the amplitudes of the pressure pulsations related to the synchronous component. At 50% load, amplitudes related to the synchronous component of the vortex rope frequency ($f^* = 0.22$) and its harmonic are approximately 0.02% of $\rho{\cdot}E$. During the start of the transient cycle, the amplitudes decrease, and, at approximately 62% load, the amplitudes increase to 0.03% of $\rho{\cdot}E$. The amplitudes of the first harmonic decrease while the amplitudes for the second harmonic increase during the transient cycle. This result indicates that the axial pressure pulsations with a frequency of 0.48 may have a stronger effect compared with that of the fundamental frequency. The similar variation was obtained with other sensors located at 90° apart. During the summation of the pressure data, pressure pulsations of second harmonic may have a similar phase and the amplitudes may increase.[53] Therefore, for reliable analysis of second harmonic,

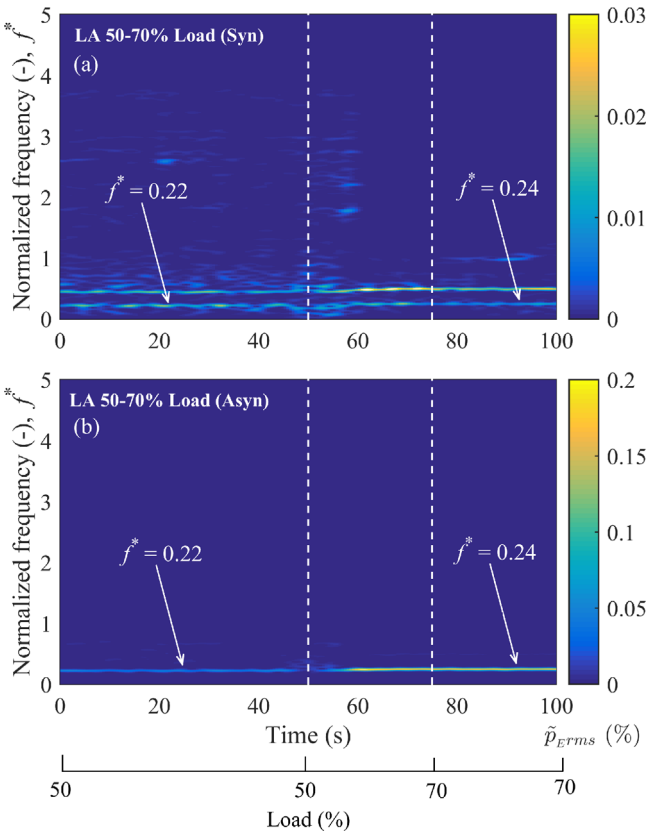

FIG. 6. Synchronous and asynchronous components of the time-series pressure pulsation acquired from S1 during load acceptance from a 50% to 70% load. The dotted lines at 50 s and 75 s indicate the time of the transient cycles. The frequencies are normalized by the runner speed 5.55 Hz. Normalized frequencies of 0.22 and 0.24 correspond to a frequency of the vortex rope in the draft turbine. The amplitudes are normalized by the reference pressure observed at the BEP: $\rho{\cdot}E = 252.17$ kPa.

two other sensors are needed on the same cross-section; in this case, sensors S2 and S4 were considered in addition to S1 and S3. Figure 6(b) presents the transient variation in the amplitude of the asynchronous pressure pulsations. A strong effect of the asynchronous pressure pulsations can be observed at both the 50% and 70% loads. The amplitudes change from approximately 0.05% to 0.2% of $\rho{\cdot}E$. No harmonic of the frequency associated with asynchronous pressure pulsations is observed. At the start of the transient cycle, the frequency of asynchronous components disappeared for a few seconds, which may be due to a sudden increase of the flow rate as the guide vanes open and may be due to a momentary increase of the axial velocity component compared with the tangential/radial velocity, which is primarily responsible for the development of vortex rope.[31]

A spectral analysis of the synchronous and asynchronous pressure pulsations during load rejection from a 100% to a 50% load is provided in Fig. 7. At a 100% load, the turbine operation is stable, and no high amplitude frequency can be observed. When the load is approximately 80%, high amplitudes of the synchronous component are observed, as indicated in Fig. 7(a). This is approximately when the turbine reached the operating point at a 70% load. The analysis for the asynchronous pressure pulsations indicated a maximum amplitude of 0.16% of the $\rho{\cdot}E$. The appearance of the asynchronous component related to a vortex rope frequency ($f^* = 0.22$) at $t = 58$ s indicates the starting of the formation of the vortex rope in the draft tube. The variation in the pressure pulsations and their amplitudes at this instant in time can be clearly observed in Fig. 2(f). After 90 s, the systematic frequency of vortex rope disappeared and the random pulsations persisted.

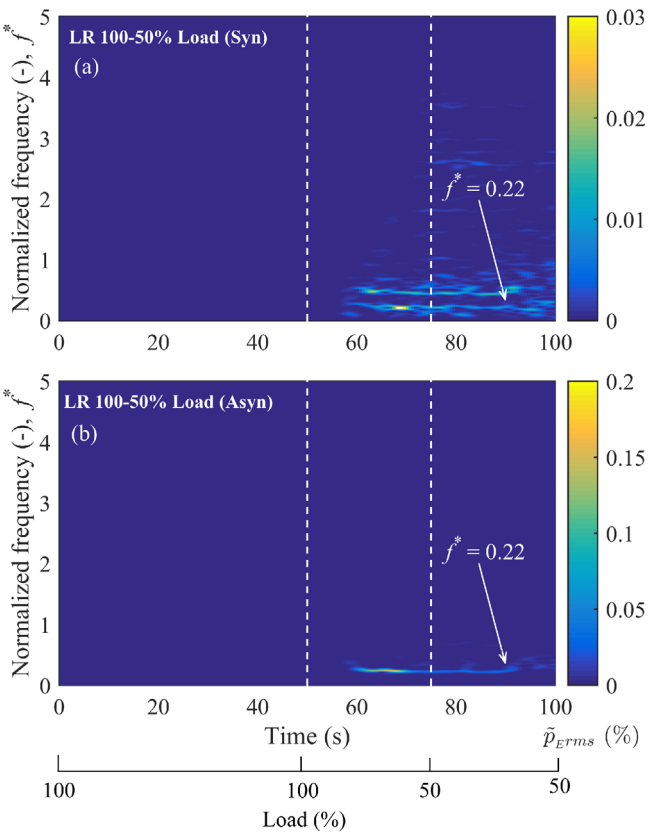

FIG. 7. Synchronous and asynchronous components of the time-series pressure pulsation acquired from S1 during load rejection from a 100% to a 50% load. The dotted lines at 50 s and 75 s indicate the time of the transient cycles. The frequencies are normalized by the runner speed 5.55 Hz. The normalized frequency of 0.22 corresponds to a frequency of the vortex rope in the draft turbine. The amplitudes are normalized by the reference pressure observed at the BEP: $\rho{\cdot}E = 252.17$ kPa.

2. Start-up

The start-up procedure of the turbine is generally defined at the time of commissioning or refurbishment, and it is followed over the service life. For the current investigation, the pressure measurements were carried out during the start-up cycle of turbine-1 and the generator synchronization at a minimum load. The pressure variation at S1 location is shown in Fig. 8. Before the start of the turbine ($t = 0$–50 s), the runner was at a standstill, the guide vanes were completely closed, and no water flow rate through the runner. The operating pressure in the draft tube before the start-up is 107.6 kPa at the measurement location. The guide vanes were opened at $t_1 = 50$ s, and the discharge to the runner increased gradually. The pressure oscillations, which occur immediately after the guide vane opens, can be observed at the measurement location. The oscillations are ± 6 kPa ($= 2.4\%$ of the operating head) of the instantaneous mean pressure value. The generator synchronization process was initiated after achieving a synchronous speed of the runner at $t_2 = 70$ s. The generator was successfully synchronized at $t = 85$ s. An unstable flow condition can be observed immediately after the generator synchronization at a 40% load (t_3). The unsteady pressure pulsations are ± 8 kPa of the instantaneous mean pressure value. A similar pressure variation was observed to occur at the other locations, S2, S3, and S4. The time-average pressure variation at S1, S2, S3, and S4 is provided in Fig. 9. The pressure values are averaged by using a window length of the samples that corresponds to one complete revolution of the runner. The oscillations in the pressure variation at all of the locations are in phase. A small asymmetry in the pressure values between the S1/S3 and S2/S4 can be observed, which could be related to the variable discharge from the blade passages during the start-up process. The frequency component and the corresponding amplitudes in the pressure pulsations are analyzed through the spectral analysis. The same window side and the overlapping factor were considered as for the load acceptance cases. Figure 10 illustrates the amplitude spectrum of the acquired pressure pulsation during the turbine start-up. The maximum amplitude is 0.1% of $\rho \cdot E$. The dimensionless frequencies observed at time t_1, t_2, and t_3 were 0.12, 0.14, and 0.32, respectively. The dimensionless frequency observed after the generator synchronization was 0.22, which corresponds to the vortex rope.

B. Pressure measurements: Turbine-2

1. Load acceptance and load rejection

Turbine-2 is horizontal-axis type and the operating head is 32.6 m. Unsteady pressure measurements have been performed during the load acceptance and start-up conditions. Three transient conditions were investigated, i.e., load acceptance from 70% to 90%, 90% to 100%, and 100% to 110%. Figure 11 depicts the acquired pressure values at the corresponding transient conditions of load acceptance. The pressure values acquired from S1 and the instantaneous mean pressure are shown. The instantaneous mean value is computed by using a moving

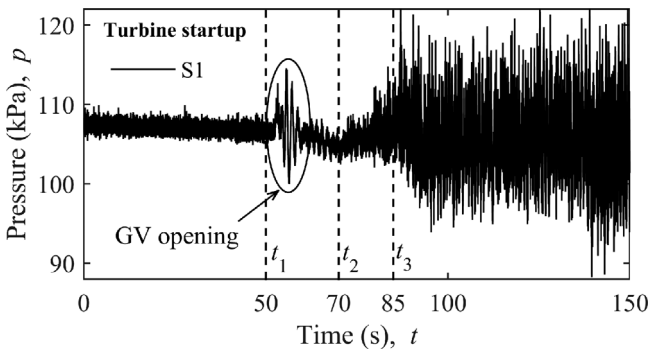

FIG. 8. Pressure variation at S1 during the turbine start-up from the standstill condition to a 40% load operating condition. The times t_1, t_2, and t_3 correspond to the guide vane opening from a completely closed position, the start of the synchronization process, and generator synchronization to the corresponding load, respectively.

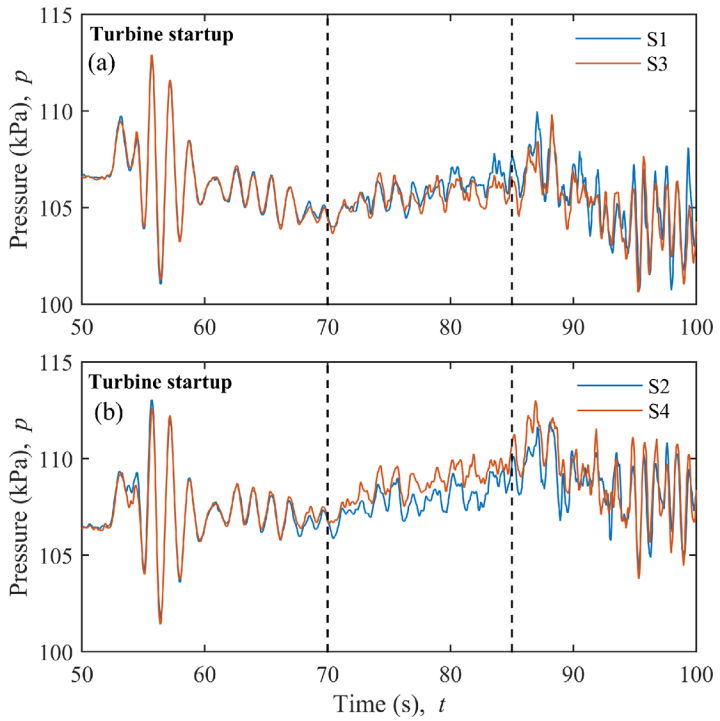

FIG. 9. Time-averaged pressure variation in the draft tube during start-up of the turbine. The pressure sensors are located at a distance of $0.27{\cdot}D$ from the runner outlet. The times of 50 s, 70 s, and 85 s correspond to the guide vane opening from a completely closed position, the start of the synchronization process, and generator synchronization to the corresponding load, respectively.

window length of 3 s. For better visualization, a zoom window of 25 s, starting from 50 s to 75 s, during load acceptance is shown next to the corresponding transient condition. The transient time is adjusted to 50 s for a comparison among the transient conditions and for a better understanding of the pressure variation. At a 70% load operating condition (before $t = 50$ s), high amplitude pressure pulsations can be observed, which correspond to a frequency of 1.69 Hz in the draft tube. During the load acceptance from a 70% to 90% load, the pressure at the measurement location decreases and stabilizes at a pressure of 40.38 kPa. From the beginning of the transient cycle ($t = 54$ s), the time of the guide vane movement was approximately 2 s.

The load acceptance from a 90% to a 100% load is presented in Fig. 11(c), and a zoom window of the transient cycle is provided in Fig. 11(d). The load was changed between 58 s

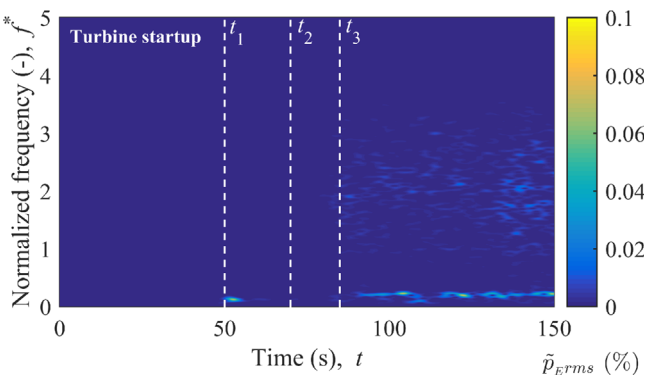

FIG. 10. Spectral analysis of the pressure pulsations acquired from S1 during the turbine start-up. The times t_1, t_2, and t_3 correspond to the guide vane opening from a completely closed position, the start of the synchronization process, and generator synchronization to the corresponding load, respectively.

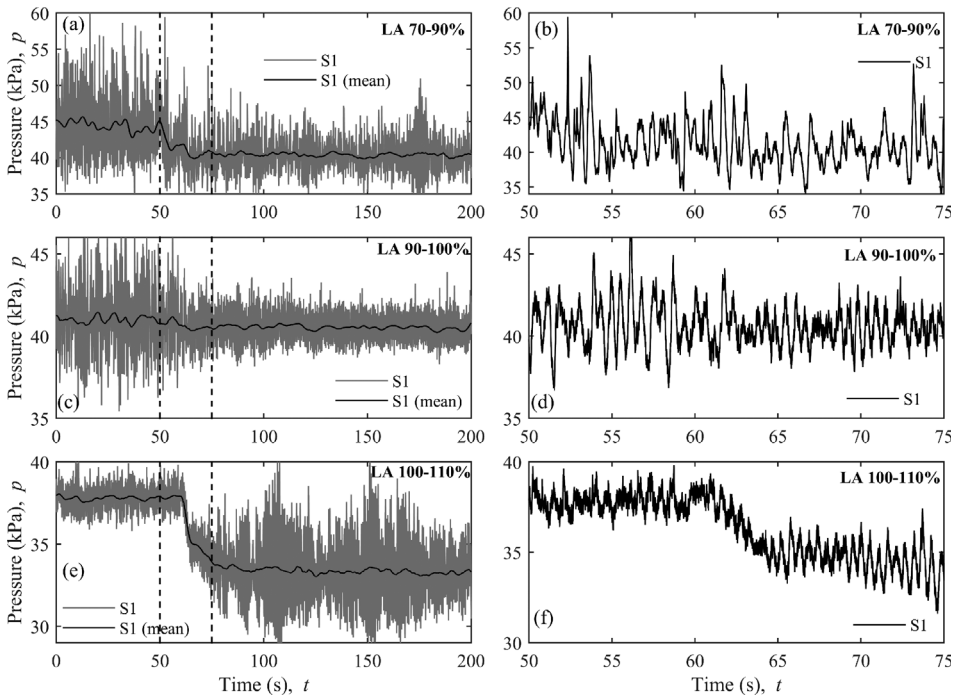

FIG. 11. Unsteady pressure variation at S1 during load acceptance of the Francis turbine-2. The figures on the left depict the acquired pressure values during the measurements and the instantaneous mean pressure. The figures on the right are the zoom-in images of the windows marked in the left-side figures from 50 s to 75 s of the corresponding transient cycle. The load acceptance from a 70% to a 110% load in 10% load increments is shown.

and 60 s. The amplitude decreases during the transition into the BEP load. The amplitude of the pressure pulsation decreased nearly two times at the BEP. A zoom window depicts a small variation in the frequency of the pressure pulsations during the transient cycle, which may be attributed to the runner frequency and other random pulsations.

The load acceptance from a 100% to a 110% load is provided in Figs. 11(e) and 11(f). The amplitude of the unsteady pressure pulsations increase as the transition into a high load occurs. The amplitude of the pressure pulsations is 2.5 times that of the amplitude observed at the BEP. The estimated standard deviation of the pressure values during the load acceptance is provided in Fig. 12. The maximum standard deviation can be observed at the 70% load operating condition, whereas the minimum standard deviation can be observed at the 100% load operating condition. During the transient cycle of the load acceptance, the standard deviation decreases as

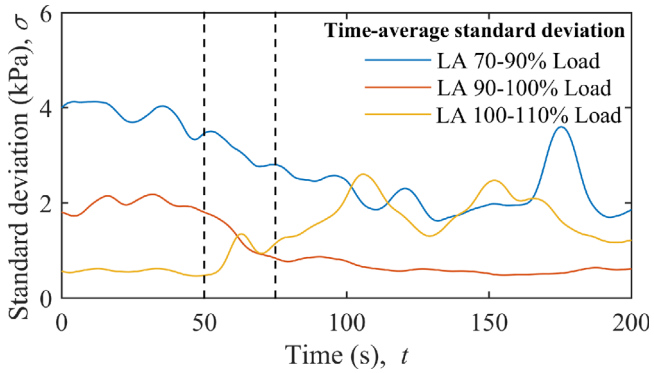

FIG. 12. Time-average standard deviation of the pressure values acquired during load acceptance of turbine-2. The dotted lines at 50 s and 75 s correspond to the transient cycle.

the load increases from 70% to 90% and 90% to 100%. The standard deviation increases when moving from a 100% to 110% load operating condition. Unlike the turbine-1, ±10% of BEP operating condition is not stable in the turbine-2 cases, in which the amplitudes of pressure pulsations are high, in addition to some random noise.

A spectral analysis of the pressure data acquired from locations S1, S2, S3, and S4 during the transient operating condition is conducted. Frequencies and amplitudes are normalized similar to the turbine-1 cases by using Eqs. (5) and (6), respectively. Figure 13 presents a spectrogram of the pressure data during load acceptance from the 70% to the 90% load operating condition. During the load change, a variation in the frequency of the vortex rope was observed from 0.27 to 0.25. A high amplitude of the dimensionless frequency of 0.27 can be observed at the 70% load operating condition. The amplitude decreases during the transient cycle. The estimated amplitudes during the transient cycle are approximately 0.045% of $\rho \cdot E$. At a 90% load, the vortex rope frequency of 0.25 is not continuous, and this may be due to the dominant effect of random pulsations as well as modulation of random frequencies around the blade-passing frequency. No other frequency was observed during the transient condition. Similarly, the variation in the frequency and amplitude during load acceptance from the 100% to the 110% load operating condition is provided in Fig. 14. At the 100% (BEP) load operating condition, the turbine was operating under stable conditions; therefore, no frequency of high amplitude is observed. A dimensionless frequency of 0.28 can be observed during the transition to the 110% load. The amplitude of this frequency gradually increases, and the maximum amplitude is 0.05% of $\rho \cdot E$. In the horizontal-axis turbine, unlike the vertical-axis turbine, the frequency of vortex rope increases as the load increases, and the increased frequency was $f^* = 0.02$ for the 20% load increase. The possible cause may be a dominant effect of tangential velocity relative to the axial and radial velocity components in this turbine. Furthermore, to investigate the synchronous and asynchronous components during the transient cycles, a spectral analysis of the pressure data acquired from locations S1 and S3 is conducted. The spectral analysis of the pressure values acquired during the load acceptance from a 70% to a 90% load is presented in Fig. 15. Low amplitudes of the synchronous components and relatively high amplitudes of the asynchronous component can be seen. The amplitudes of the synchronous component at the 70% load condition are lower than that of the asynchronous component. At the 90% load operating condition, the amplitudes are increased by 12%. Interestingly, the frequency of asynchronous component observed at the 70% load is diminished at the 90% load operating condition. This result indicates that only the axial pressure pulsations exist at the 90% load operating condition. It seems that the runner axis and the draft tube orientation play a dominant role in the development of the synchronous/asynchronous pulsations.[54] In this turbine, the draft tube

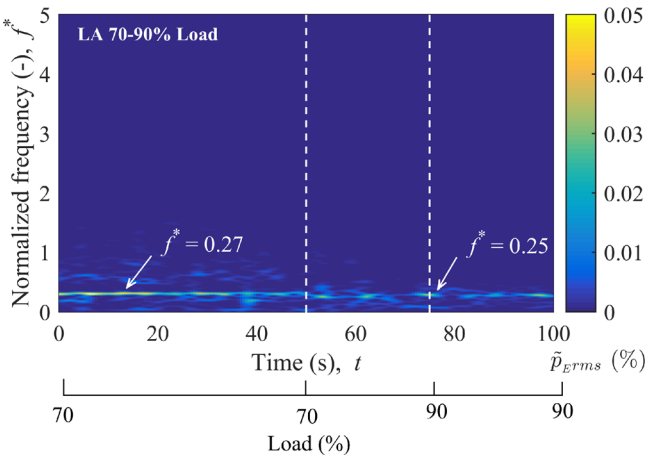

FIG. 13. A spectrogram of the time-series pressure pulsation at S1 during the load acceptance from a 70% to 90% load. The dotted lines at 50 s and 75 s indicate the time of the transient cycles. The frequencies are normalized by the runner's angular speed of 6.25 Hz. The amplitudes are normalized by the reference pressure observed at the BEP: $\rho \cdot E = 319.8$ kPa.

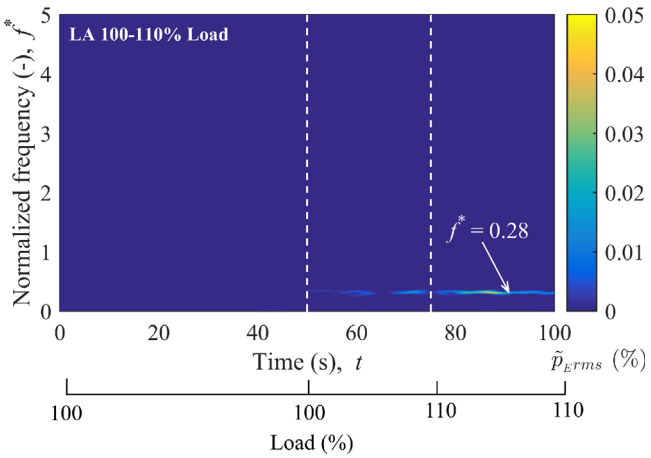

FIG. 14. A spectrogram of the time-series pressure pulsation at S1 during load acceptance from a 100% to a 110% load. The dotted lines at 50 s and 75 s indicate the time of the transient cycles. The frequencies are normalized by the runner's angular speed of 6.25 Hz. The amplitudes are normalized by the reference pressure observed at the BEP: $\rho \cdot E = 319.8$ kPa.

outlet is oriented downward from the elbow (see Fig. 1), the effect of asynchronous-type pressure waves developed between the elbow and the draft turbine outlet may be confined to that conduit area and not reaching to the runner outlet-measurement plane. Furthermore, magnitudes of tangential velocity at 90% load may not be sufficient to develop spiral vortex.

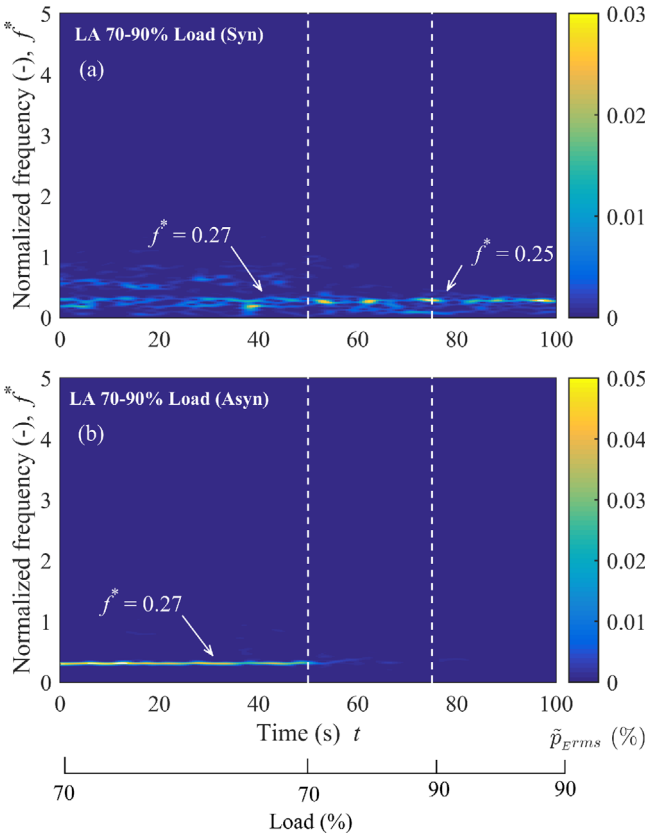

FIG. 15. Synchronous and asynchronous components of the time-series pressure pulsation acquired from S1 during the load acceptance from a 70% to a 90% load. The dotted lines at 50 s and 75 s indicate the time of the transient cycles. The frequencies are normalized by the runner's angular speed of 6.25 Hz. The normalized frequencies of 0.25 and 0.27 correspond to a frequency of the vortex rope in the draft turbine. The amplitudes are normalized by the reference pressure observed at the BEP: $\rho \cdot E = 319.8$ kPa.

Spectral analysis of the pressure values acquired from locations S1 and S3 is shown in Fig. 16. Pressure data are extracted for 2 s from the start of the guide vane opening. The pressure sensors S1 and S3 were located at radial positions 180° from each other on the same plane. Location S1 was below the horizontal plane passing through the axis of the runner, and location S3 was above the horizontal plane. Therefore, a low amplitude at location S3 was expected, which can be observed by comparing the amplitude of the vortex breakdown frequency of 0.27 in Figs. 16(a) and 16(b). Equations (7) and (8) were used to estimate the synchronous and asynchronous components of the pressure pulsations, respectively. The amplitude of the synchronous component was almost identical to the amplitude observed at locations S1 and S3. The amplitude of the asynchronous component was reduced by 50%, indicating that the synchronous component had a large effect on the draft tube flow during the first 2 s of load change. The large effect may be attributed to an increase of axial velocity as discharge to the draft tube increases. Pressure waves travelling between the runner outlet and the draft tube may have a dominant effect on the unsteady pressure field.

2. Start-up

Before turbine start-up, the main inlet valve was located before the spiral casing inlet was opened. Once the pressure was stabilized in the turbine, the guide vanes opened, and water flowed to the runner. The guide vanes were opened until the runner achieved a synchronous speed of 6.25 rps. After achieving a stable speed of the runner and a stable torque value, the

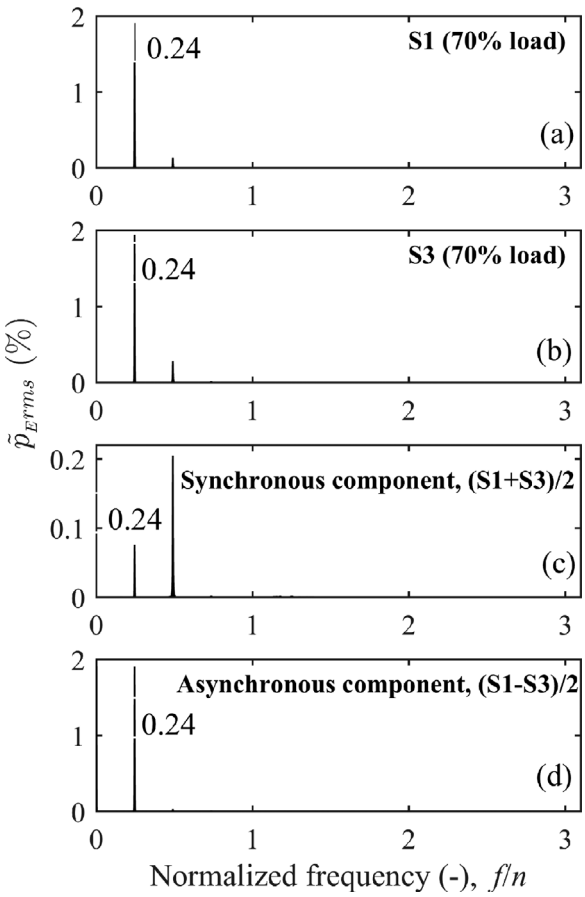

FIG. 16. Spectral analysis of pressure signals S1 and S3 located at radial positions 180° from each other. The synchronous component of the pressure pulsations is computed as (S1 + S2)/2, and the asynchronous component is computed as (S1 − S2)/2. The maximum amplitude spectrum is 0.3% of $\rho \cdot E$. The peak at $f/n = 0.27$ corresponds to the frequency of the vortex breakdown at the measurement location.

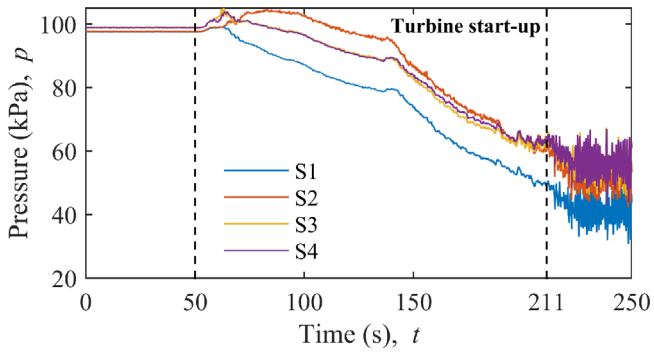

FIG. 17. Pressure variation during the turbine start-up from a standstill condition to a 40% load operating condition. The times of 50 s and 211 s correspond to the guide vane opening from a completely closed position and generator synchronization to no load, respectively.

generator was connected to the grid. The power output was increased by further opening the guide vanes. Figure 17 presents the pressure variation during the start-up cycle of turbine-2. The guide vane was adjusted to open to 50 s during the start-up cycle. At 50 s, the guide vanes were opened, discharge to the runner was initiated, and the runner was set to spin. The generator was synchronized to the power grid at 211 s. After the synchronization, the pressure pulsations in the draft tube dramatically increased. The turbine was operating at a no-load condition, and, after completing the synchronization process, the guide vanes were opened further, while the power output increased to a 40% load. During the start-up cycle, pressure in the draft tube changed from 97.5 kPa to 42.9 kPa. Figure 18 presents an estimated standard deviation of the fluctuating pressure values acquired during the turbine start-up. The standard deviation is estimated by using the samples acquired during 1 s, i.e., moving window size and 80% overlap. The value of the standard deviation between 50 s and 211 s is low (<0.8 kPa). However, after the generator synchronization, the standard deviation increases rapidly, over the mean value of 6 kPa. The turbine was operating under a no-load condition, and the discharge was varied. This resulted in high amplitude pressure pulsation in the draft tube.[55,56] Figure 19 presents the spectral analysis of the pressure values acquired from S1 during the start-up cycle. No frequency of high amplitude was observed before the generator synchronization. Immediately after the generator synchronization, a high amplitude frequency of 1.02 Hz, which corresponded to a dimensionless frequency of 0.16, was observed. The frequency seems to be associated with an instable flow condition in the draft tube developed during the no-load condition.[56] The amplitudes correspond to the synchronous pressure pulsations. No pressure pulsations related to the asynchronous component were observed between 211 s and 250 s, i.e., a 0% to a 40% load. Under this condition, the discharge to the turbine was low, and the runner rotational speed was

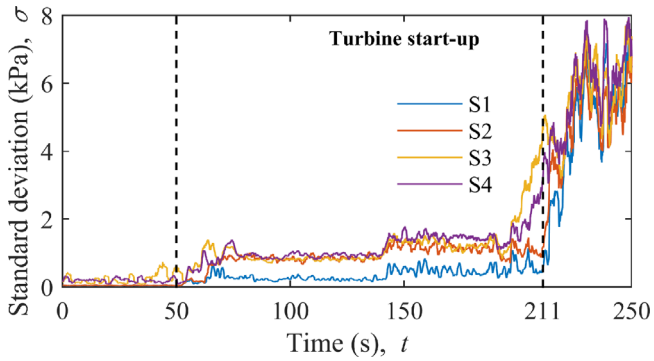

FIG. 18. Standard deviation of the unsteady pressure pulsations acquired during the turbine start-up and the generator synchronization. The dotted lines at 50 s and 211 s indicate the time that the guide vanes open and the generator synchronization at no load, respectively.

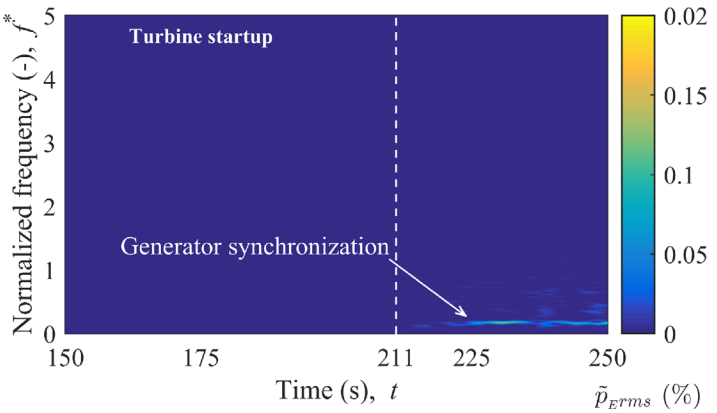

FIG. 19. Spectral analysis of the pressure pulsations acquired during the start-up cycle of turbine-2. The maximum amplitudes are 0.2% of $\rho{\cdot}E$. The dotted line at 211 s indicates the start time of the generator synchronization at no load.

high, and the runner rotational speed was high, i.e., runaway speed, for the given guide vane opening angle.

IV. CONCLUSIONS

Unsteady pressure measurements were performed on two Francis turbine prototypes (specific speed = 0.27). Turbine-1 was a vertical-axis type and the operating head was 25.7 m; whereas, turbine-2 was a horizontal-axis type and the operating head was 32.6 m. The measurements were performed during transient conditions, such as load acceptance, load rejection, and start-up. Four pressure sensors were mounted in the draft tube cone to acquire unsteady pressure data. A detailed analysis of the acquired pressure values was performed, including the computation of the spectral content, standard deviation, and components of the vortex rope frequency.

At a 50% load, the random pulsations were dominant; whereas, at 70% load systematic pulsations, vortex rope and rotor stator interaction, were dominant. Amplitudes of random pulsations at 50% load were up to five times than those at a 100% (BEP) load. Amplitudes of vortex rope frequency were maximum at a 70% load for both turbines. The vortex rope frequency at a 50% load was found to be changing from $f^* = 0.22$ to 0.24 as the load changed to 70%. The development of the vortex rope during the load acceptance from stable operating loads to partial loads was observed through the variation in pressure amplitudes and frequency. Amplitudes related to the asynchronous component were significantly low (<0.03% of $\rho{\cdot}E$) compared with the synchronous component (<0.2% of $\rho{\cdot}E$). The amplitudes of the first harmonic reduced while the amplitudes of the second harmonic increased during the load change from 50% to 70%. In the vertical-axis turbine, amplitudes of asynchronous pressure pulsations were 20 times larger than those of the synchronous component; whereas, in the horizontal-axis turbine, amplitudes of asynchronous pressure pulsations were two times smaller than those of the synchronous component.

In the horizontal-axis turbine, unlike the vertical-axis turbine, the frequency of the vortex rope increases as the load increases, and the increased frequency was $f^* = 0.02$ for the 20% load increase. The possible cause may be a dominant effect of tangential velocity relative to the axial and radial velocity components in this turbine. In the horizontal-axis turbine, interestingly, the frequency of asynchronous component observed at the 70% load is diminished at the 90% load operating condition. It seems that the runner axis and the draft tube orientation play a dominant role in the development of the synchronous/asynchronous pulsations. In this turbine, the draft tube outlet is oriented downward from the elbow, the effect of asynchronous-type pressure waves developed between the elbow and the draft turbine outlet may be confined to that conduit area and not reaching to the runner outlet–measurement plane. Furthermore, magnitudes of tangential velocity at the 90% load may not be sufficient to develop spiral vortex.

During the start-up cycle, a variable pressure along the draft tube circumference was observed. High amplitude pressure fluctuations were obtained when the guide vanes were opened from a close position and the generator was synchronized to the power grid. The amplitudes were up to 3.5% of the operating head. Furthermore, at no load after synchronization, the amplitudes were consistent and the random pulsations were dominant. However, there was no indication of pulsation related to vortex rope–blade passing frequency. The frequency of random pulsations was varied from 1 Hz to 7 Hz in both of the turbines. During turbine start-up when the generator synchronizes the load, the pressure amplitudes in the draft tube significantly increase for a short time, which are 2.8 times the BEP. This may be one of the key damaging events of a turbine, when fatigue loading and stresses on the runner blades may be high.

During the transient cycle of load acceptance, amplitudes of pressure fluctuations were found to be 1.6 times that of the steady-state load, particularly for the cases of a 50%–70% load change and a 100%–50% load in the vertical-axis turbine. The high amplitudes were observed, especially immediately after the start of the guide vane opening and closing from the steady condition. While changing the load around the BEP $\pm$ 10% of BEP, the instantaneous amplitudes were nearly similar to that of the steady-state load. Investigations of the horizontal-axis turbine revealed high amplitude fluctuations during the load change from 70% to 90% and 90% to 100%. The amplitudes are almost two times that of the steady-state condition. Unlike the vertical-axis turbine, $\pm$10% of the BEP operating condition is not stable in the horizontal-axis turbine, where the amplitudes of pressure pulsations are high in addition to some random noise.

ACKNOWLEDGMENTS

The presented work was conducted under a research project titled "Efficiency Measurement at Leirfossen Kraftverk." This project was financially supported by Statkraft AS, Norway. The low-head Francis turbines located at Nedre Leirfossen and Øvre Leirfossen were investigated. Furthermore, hydraulic efficiency measurements and unsteady pressure measurements were performed.

NOMENCLATURE

asyn	asynchronous
BEP	best efficiency point
D	runner outlet diameter (m)
E	specific hydraulic energy (J kg^{-1})
f	frequency (Hz)
f^*	normalized frequency (-)
GV	guide vane
H	head (m)
LA	load acceptance
LR	load rejection
n	runner angular speed (rps)
N_{QE}	specific speed (-)
nED	speed factor (-)
p	pressure (kPa)
P	power (MW), signal power (dB)
Q	discharge (m3 s^{-1})
QED	discharge factor (-)
RMS	root mean square
rps	revolutions per second
syn	synchronous
S1, S2, S3, and S4	locations of pressure sensors mounted in a draft tube cone
t	time (s)

Greek letters

ρ water density (kg m^{-3})
σ standard deviation (kPa)

[1]G. Caralis, D. Papantonis, and A. Zervos, Renewable Sustainable Energy Rev. **16**(5), 2558–2565 (2012).
[2]J. Hell, in *HYPERBOLE, Porto, Portugal* (2017), p. 7.
[3]C. Trivedi, E. Agnalt, and O. G. Dahlhaug, Renewable Energy **113**, 397–410 (2017).
[4]O. Nilsson and D. Sjelvgren, IEEE Trans. Power Syst. **12**(1), 38–44 (1997).
[5]M. Gagnon, J. Nicolle, J. F. Morissette, and M. Lawrence, IOP Conf. Ser.: Earth Environ. Sci. **49**(5), 052005 (2016).
[6]M. Coulaud, R. Fraser, J. Lemay, P. Duquesne, V. Aeschlimann, and C. Deschênes, IOP Conf. Ser.: Earth Environ. Sci. **49**(6), 062024 (2016).
[7]K. Amiri, B. Mulu, M. J. Cervantes, and M. Raisee, Int. J. Fluid Mach. Syst. **9**(2), 182–193 (2016).
[8]C. Trivedi, J. Fluids Eng. **140**(1), 011101 (2017).
[9]C. Trivedi, B. Gandhi, M. Cervantes, and O. Dahlhaug, Renewable Energy **83**, 828–836 (2015).
[10]C. Trivedi, M. Cervantes, O. Dahlhaug, and B. Gandhi, J. Fluids Eng. **137**(6), 061106 (2015).
[11]W. C. Guo, J. D. Yang, J. P. Chen, Z. Y. Peng, Y. Zhang, and C. C. Chen, IOP Conf. Ser.: Earth Environ. Sci. **49**(5), 052016 (2016).
[12]M. Gagnon, N. Jobidon, M. Lawrence, and D. Larouche, IOP Conf. Ser.: Earth Environ. Sci. **22**, 032022 (2014).
[13]C. Trivedi, M. Cervantes, B. Gandhi, and O. Dahlhaug, J. Hydraul. Res. **52**(2), 283–297 (2014).
[14]C. Trivedi, M. Cervantes, B. Gandhi, and O. Dahlhaug, J. Hydrodyn., Ser. B **26**(2), 277–290 (2014).
[15]B. Nennemann, J. F. Morissette, J. Chamberland-Lauzon, C. Monette, O. Braun, M. Melot, A. Coutu, J. Nicolle, and A. M. Giroux, IOP Conf. Ser.: Earth Environ. Sci. **22**, 032055 (2014).
[16]C. Trivedi, B. Gandhi, and M. Cervantes, J. Hydraul. Res. **51**(2), 121–132 (2013).
[17]T. Kolšek, J. Duhovnik, and A. Bergant, J. Hydraul. Res. **44**(1), 129–137 (2006).
[18]M. Melot, C. Monette, A. Coutu, and B. Nenneman, in *Hydro 2013, Innsbruck, Austria* (2013), p. 8.
[19]P. Côté, G. Dumas, E. Moisan, and G. Boutet-Blais, IOP Conf. Ser.: Earth Environ. Sci. **22**, 032023 (2014).
[20]C. Trivedi, Eng. Failure Anal. **77**, 1–22 (2017).
[21]C. Trivedi and M. Cervantes, Renewable Sustainable Energy Rev. **68**(1), 87–101 (2017).
[22]H.-J. Huth, Ph.D. thesis, Norwegian University of Science and Technology (NTNU) (2005).
[23]A. I. Bosioc, R. Susan-Resiga, S. Muntean, and C. Tanasa, J. Fluids Eng. **134**(8), 081104 (2012).
[24]Z. W. Wang and L. J. Zhou, J. Fluids Eng. **128**(4), 649–655 (2006).
[25]P. Dörfler, M. Sick, and A. Coutu, *Flow-Induced Pulsation and Vibration in Hydroelectric Machinery: Engineer's Guidebook for Planning, Design and Troubleshooting*, 1st ed. (Springer-Verlag, London, 2013).
[26]R. Jester-Zuerker, A. Jung, and M. Maiwald, IOP Conf. Ser.: Earth Environ. Sci. **15**, 062010 (2012).
[27]P. P. Jonsson, B. G. Mulu, and M. J. Cervantes, Appl. Energy **94**, 71–83 (2012).
[28]H. Foroutan and S. Yavuzkurt, J. Appl. Mech. **81**(6), 061011 (2014).
[29]H. Foroutan and S. Yavuzkurt, J. Appl. Mech. **81**(6), 061010 (2014).
[30]R. Goyal, M. J. Cervantes, and B. K. Gandhi, Int. J. Fluid Mach. Syst. **10**(2), 164–175 (2017).
[31]R. Goyal, M. J. Cervantes, and B. K. Gandhi, J. Fluids Eng. **139**(4), 041102 (2017).
[32]A. A. Gavrilov, A. V. Sentyabov, A. A. Dekterev, and K. Hanjalić, "Vortical structures and pressure pulsations in draft tube of a Francis-99 turbine at part load: RANS and hybrid RANS/LES analysis," Int. J. Heat Fluid Flow **63**, 158–171 (2017).
[33]G. K. Rajan and J. M. Cimbala, J. Fluids Eng. **139**(2), 021102 (2016).
[34]G. D. Ciocan, M. S. Iliescu, T. C. Vu, B. Nennemann, and F. Avellan, J. Fluids Eng. **129**(2), 146–158 (2007).
[35]A. Favrel, A. Müller, C. Landry, K. Yamamoto, and F. Avellan, Exp. Fluids **56**(12), 1–15 (2015).
[36]C. Trivedi, M. Cervantes, and O. G. Dahlhaug, Energies **9**(2), 74 (2016).
[37]M. J. Cervantes, C. H. Trivedi, O. G. Dahlhaug, and T. Nielsen, J. Phys.: Conf. Ser. **579**, 011001 (2015).
[38]M. J. Cervantes, C. Trivedi, O. G. Dahlhaug, and T. Nielsen, J. Phys.: Conf. Ser. **782**, 011001 (2017).
[39]W. Zeng, J. Yang, R. Tang, and W. Yang, Renewable Energy **99**, 35–44 (2016).
[40]H. Ramos and A. B. Almeida, J. Hydraul. Res. **39**(4), 429–436 (2001).
[41]C. Chen, C. Nicolet, K. Yonezawa, M. Farhat, F. Avellan, and Y. Tsujimoto, J. Fluids Eng. **130**(4), 041106 (2008).
[42]X. Escaler, J. V. Ekanger, H. H. Francke, M. Kjeldsen, and T. K. Nielsen, J. Fluids Eng. **137**(1), 011103 (2014).
[43]A. Favrel, C. Landry, A. Müller, K. Yamamoto, and F. Avellan, IOP Conf. Ser.: Earth Environ. Sci. **22**, 032035 (2014).
[44]J. Arpe, C. Nicolet, and F. Avellan, J. Fluids Eng. **131**(8), 081102 (2009).
[45]T. S. Lee and S. Pejovic, J. Fluids Eng. **118**(4), 706–709 (1996).
[46]S. Pejovic and B. Karney, IOP Conf. Ser.: Earth Environ. Sci. **22**, 042006 (2014).
[47]IEC 60193, *International Standard* (International Electrotechnical Commission, Geneva, Switzerland, 1999), Vol. IEC60193, p. 578.
[48]G. J. Dolecek, *Random Signals and Processes Primer with Matlab* (Springer, New York, 2013).
[49]P. O'Shea, A. Z. Sadik, and Z. M. Hussain, *Digital Signal Processing: An Introduction with MATLAB and Applications* (Springer, Berlin, Heidelberg, 2011).
[50]T. Jacob, Ph.D. thesis, Ecode Polytechnique Federale de Lausanne (1993).
[51]T. Jacob and J.-E. Prénat, in *Proceedings of the XVIII IAHR Symposium on Hydraulic Machinery and Cavitation*, edited by E. Cabrera, V. Espert, and F. Martínez (Springer, Dordrecht, Netherlands, 1996), pp. 855–864.
[52]P. Doerfler and N. Ruchonnet, IOP Conf. Ser.: Earth Environ. Sci. **15**, 062002 (2012).
[53]R. Goyal, C. Trivedi, B. K. Gandhi, C. J. Michel, and G. Ole Dahlhaug, Sadhana **41**(11), 1311–1320 (2016).
[54]M. Nishi and S. Liu, Int. J. Fluid Mach. Syst. **6**(1), 33–48 (2013).
[55]C. Mende, W. Weber, and U. Seidel, IOP Conf. Ser.: Earth Environ. Sci. **49**(6), 062017 (2016).
[56]Z. Li, H. Bi, Z. Wang, and Z. Yao, Proc. Inst. Mech. Eng. Part A **230**(6), 570–585 (2016).